Enhanced optical properties of $Si_{1-x}Ge_x$ alloy nanocrystals in a planar microcavity

Kimiaki Toshikiyo
Graduate School of Science and Technology, Kobe University, Rokkodai, Nada, Kobe 657-8501, Japan

Minoru Fujii[a] and Shinji Hayashi
Department of Electrical and Electronics Engineering, Faculty of Engineering, Kobe University, Rokkodai, Nada, Kobe 657-8501, Japan

(Received 3 September 2002; accepted 22 November 2002)

The emission properties of $Si_{1-x}Ge_x$ alloy nanocrystals (nc-$Si_{1-x}Ge_x$) in an optical microcavity were studied, and the results were compared with those of nc-Si in the same structure. The cavity consists of two distributed Si/SiO_2 Bragg reflectors (DBRs) sandwiching a thin SiO_2 film containing nc-$Si_{1-x}Ge_x$. The commonly observed cavity effects, that is, spectral narrowing, high directionality, and photoluminescence (PL) enhancement in the normal direction, were observed. In nc-$Si_{1-x}Ge_x$, PL lifetime was lengthened by cavity formation, while that of nc-Si was shortened. This difference is due to the different dielectric contrast between active layers and DBRs. © *2003 American Institute of Physics.* [DOI: 10.1063/1.1539289]

I. INTRODUCTION

During the past decade, nanometer-sized Si and Ge crystals (nc-Si and nc-Ge) have been extensively studied because they offer new possibilities for indirect band-gap semiconductors as new materials in photoelectronic applications. It has been demonstrated that the photoluminescence (PL) energy of nc-Si is tunable from the bulk band gap to the visible region by simply controlling its size.[1–6] The tuning range can be expanded by $Si_{1-x}Ge_x$ alloy formation, because the band gap (luminescence) energy of nanometer-sized $Si_{1-x}Ge_x$ alloy crystals (nc-$Si_{1-x}Ge_x$) changes from the widened bandgap of nc-Si to that of nc-Ge depending on x.[7–10] The wide tunability of PL peak energy prompts great interest in the development of Si-based light-emitting devices.

The emission properties of such materials can be further improved by constructing a microcavity structure; that is, putting an active layer into two distributed Bragg reflectors (DBRs). When a phonon is confined in a microcavity in resonance with the emission of the active medium, the light emission becomes spectrally sharp and is strongly enhanced in the direction of confinement.[11–17]The emission energy can be tuned by properly choosing the parameters of Bragg reflectors and the thickness of the active region.

In this article, we report our study of the PL properties of nc-$Si_{1-x}Ge_x$ in a microcavity, and compare those properties with those of nc-Si in the same structure. We will show that, although the PL properties of nc-$Si_{1-x}Ge_x$ and nc-Si samples are modified in a very similar way by microcavity formation, different effects appear for PL decay dynamics. We will discuss how the dielectric contrast between an active layer and the surrounding DBRs affects PL decay dynamics.

[a]Author to whom correspondence should be addressed; electronic mail: fujii@eedept.kobe-u.ac.jp

II. EXPERIMENT

The active layer of our microcavity is a SiO_2 thin film containing either nc-Si or nc-$Si_{1-x}Ge_x$. The Bragg reflectors on top and bottom of the active layers are pairs of Si and SiO_2 layers, repeated three times. The thicknesses of the Bragg reflectors and the active layer were chosen to be $\lambda_c/4n$ and λ_c/n, respectively, where λ_c is the wavelength of the resonance and n is the reflective index of the medium. The thicknesses and refractive indexes of the layers are summarized in Table I. The refractive index values of the active layers (n_c) were estimated by spectroscopic ellipsometry.

A multitarget sputtering apparatus was used to deposit multilayer films.[6–10] The layers of Bragg reflectors were deposited by alternately operating Si or SiO_2 sputtering guns, while active layers were deposited by operating Si, Ge, and SiO_2 guns simultaneously (in the case of nc-Si, Si, and SiO_2 guns). The sputtering rate of each gun was independently controlled by adjusting the sputtering power and the distance between sputtering targets and substrates. After the deposition of a microcavity structure on a fused quartz substrate, the film was annealed in an N_2 gas atmosphere for 30 min at 1100°C. During the annealing, either nc-Si or nc-$Si_{1-x}Ge_x$ was grown in a SiO_2 matrix. The cross section of the cavity structure was examined by using a high-resolution transmission electron microscope (HRTEM). In Fig. 1(a), the cross section of a sample is shown. We can see that the Si/SiO_2 interfaces are rather smooth, with less than 10 nm of roughness. Figure 1(b) shows a HRTEM image of an active layer containing nc-$Si_{1-x}Ge_x$. Spherical nanocrystals as small as 4–5 nm in diameter were grown in amorphous SiO_2 matrices. The formation of $Si_{1-x}Ge_x$ alloy was confirmed by electron diffraction and Raman spectroscopy.[7]

PL spectra were measured with a single monochromator equipped with a liquid-N_2-cooled Ge detector. The excitation source was the 488.0-nm line of an Ar-ion laser. The angle of incident beam was about 45° from the surface of the

TABLE I. Growth parameters and refractive index data of two microvcavities. l_H and l_L are the thicknesses of the various layers of the DBR. Here, n_H, n_L, and n_c refer to the refractive index values for the high- and low-refractive index layers, (Si and SiO_2) (Ref. 17), and the central layer, respectively, and λ_c is the PL peak wavelength.

	l_H (nm)	l_L (nm)	n_H	n_L	n_c	λ_c (nm)
nc-Si	61	149	3.56	1.45	1.70	867
nc-$Si_{0.9}Ge_{0.1}$	66	162	3.56	1.45	2.18	940

sample, and PL emitted perpendicular to the surface was detected. The solid angle for the collection of emitted light was less than $1\times10^{-3}\pi$ sr. For time-response measurements, a near-infrared photomultiplier with an $InP/In_xGa_{1-x}As$ photocathode was used with a photon-counting mode. The overall time resolution of the system was about 40 ns.

III. RESULTS AND DISCUSSION

Figure 2(a) shows a reflectivity spectrum of a DBR at room temperature. A high reflectivity region (stop band) appears between 1.1 and 1.7 eV. Putting SiO_2 layers containing *nc*-Si [Fig. 2(b)] and *nc*-$Si_{1-x}Ge_x$ [Fig. 2(c)] into two DBRs causes dips (resonant peaks) to appear in the high-reflectance stop band. The energy and the linewidth of the resonant peaks are 1.43 eV and 17 meV, respectively, for *nc*-Si, and 1.32 eV and 16 meV, respectively, for *nc*-$Si_{0.9}Ge_{0.1}$.

Figures 3(a) and 3(b) show PL spectra of *nc*-Si and *nc*-$Si_{0.9}Ge_{0.1}$, respectively, obtained in the direction normal to the sample surfaces. Dashed curves represent the spectra without DBRs. The PL bandwidths (full widths at half maximum) are 315 meV for *nc*-Si, and 345 meV for *nc*-$Si_{0.9}Ge_{0.1}$. The PL spectra are narrowed down to 17 meV for *nc*-Si, and 16 meV for *nc*-$Si_{0.9}Ge_{0.1}$, by microcavity structure formation. The quality factors (Q) are 87 and 85, respectively. Furthermore, PL intensity is enhanced by a factor of about 20. The net enhancement is about 122 for both samples because a part of the excitation light is lost by the top DBR.

The enhancement of the luminescence intensity at the resonance wavelength is observed only in the normal direction, while the intensity is suppressed in other direction. This

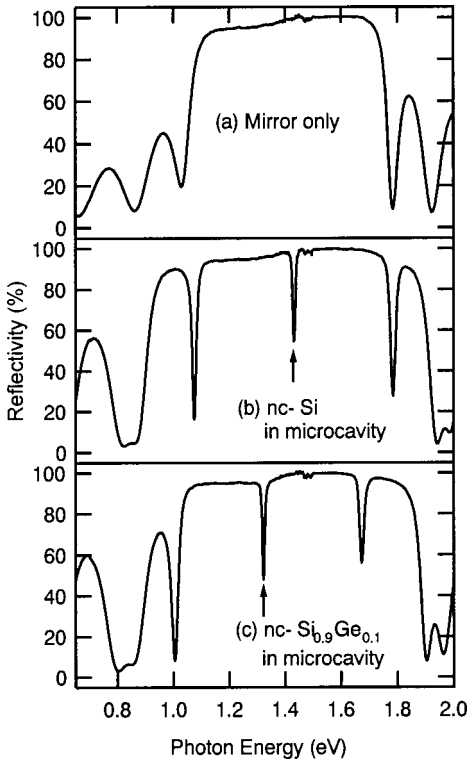

FIG. 2. Reflectivity spectra of (a) DBR, (b) *nc*-Si, and (c) *nc*-$Si_{0.9}Ge_{0.1}$ in microcavities at room temperature. For the sample having cavity structure, the sharp dips (arrows) appear in the high reflectance stop band.

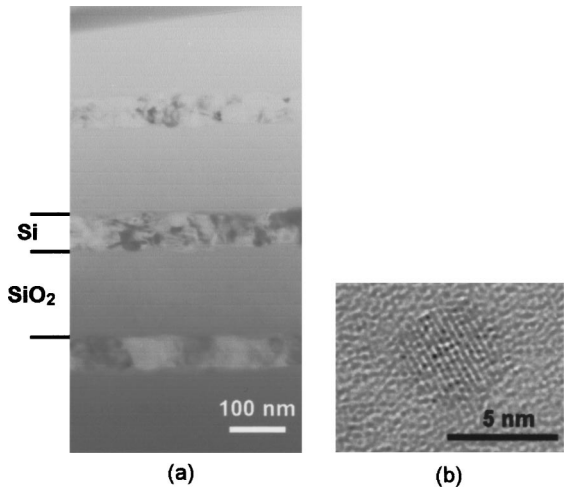

FIG. 1. Cross-sectional HRTEM image of a microcavity, which consists of (a) two distributed Si/SiO_2 Bragg reflectors and (b) a central active layer with *nc*-$Si_{1-x}Ge_x$.

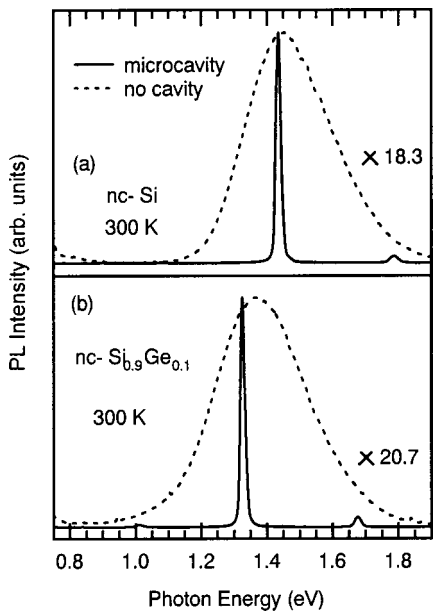

FIG. 3. PL from (a) *nc*-Si and (b) *nc*-$Si_{0.9}Ge_{0.1}$ in microcavities at room temperature. PL spectra without DBRs are broad (dashed curve). By microcavity structure formation, PL spectra are narrowed drastically (solid curve).

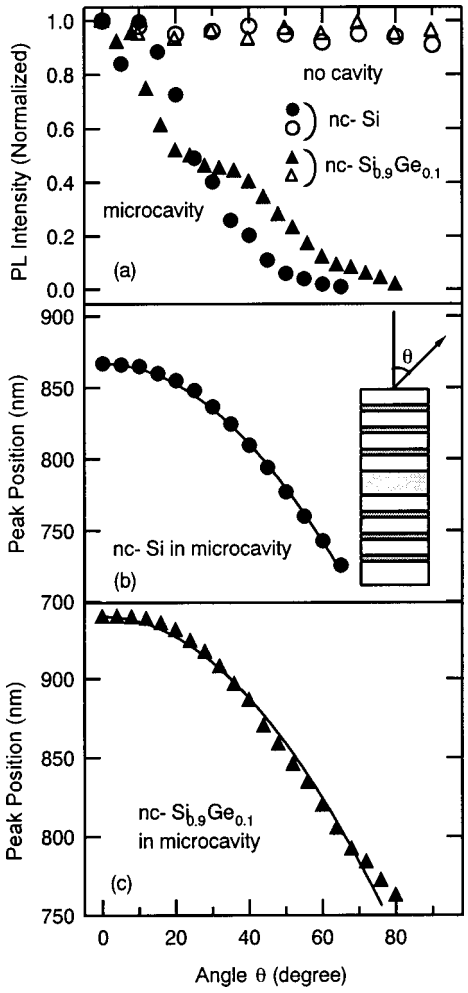

FIG. 4. (a) Integrated PL intensity, and (b) and (c) wavelength peak position as a function of detection angle with respect to the normal direction.

redistribution of the emission is a well-known cavity effect.[11–16] The enhancement value in the normal direction can be calculated from the finesse of the cavity, if reflectivity of top and bottom DBRs are high enough.[18] For δ-function-like emission spectra occurring at the resonance wavelength of the cavity, the peak intensity enhancement factor G compared to an emitter without mirrors is

$$G=\frac{\zeta}{2}\frac{(1+\sqrt{R_{\text{bottom}}})^2(1-R_{\text{top}})}{(1-\sqrt{R_{\text{top}}R_{\text{bottom}}})^2}\frac{\tau_{\text{cav}}}{\tau_{\text{act}}}, \tag{1}$$

where ζ is an antinode enhancement factor depending on the position of an active region in an electric field antinode of the cavity standing wave. This value is nearly 1 due to a thick active region. The R_{top} and R_{bottom} are the calculated reflectivities of the top and bottom DBRs; the R_{top} and R_{bottom} are 98.1% and 98.5% for nc-Si, respectively, and 97.3% and 98.4%, respectively, for nc-$Si_{0.9}Ge_{0.1}$. The τ_{cav} and τ_{act} are the respective PL lifetimes with and without the cavity. The calculated G is 120.5 for nc-Si, and 122.4 for nc-$Si_{0.9}Ge_{0.1}$. These values are very close to those observed.

Figure 4(a) shows the angle dependence of PL intensities for our microcavity structures and bare films. In microcavity structures, PL is strongly directed along the optical axis of the cavity. The PL intensities are the maximum at normal to the surface ($\theta=0°$) and then decrease rapidly with increases in the detection angle. On the other hand, for noncavity structures, the intensities are almost constant over the entire detection angle range. Figures 4(b) and 4(c) show the angle dependences of the PL peak wavelengths for nc-Si and nc-$Si_{0.9}Ge_{0.1}$, respectively. For off-normal angles, the emission wavelength shifts toward a shorter wavelength. The degree of the wavelength shift obeys a cosine of the internal cavity angle, which is approximated by the detection angle (θ) divided by the average cavity refraction index (n_{eff}). The PL peak wavelength can thus be expressed approximately as $\lambda=\lambda_c\cos(\theta/n_{\text{eff}})$. [12] By fitting the experimental results to this formula, n_{eff} can roughly be estimated. The estimated values are 1.9 for nc-Si and 2.1 for nc-$Si_{0.9}Ge_{0.1}$.

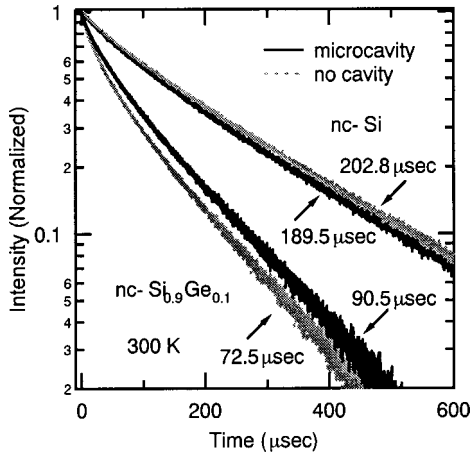

FIG. 5. Room-temperature time decay of the PL for the microcavities (solid curve) and the non-cavities (dashed curve).

Figure 5 shows PL decay curves detected at the PL maximum. The decay curves are nonexponential. Nonexponential decay curves are commonly observed for similar systems.[7] The PL decay of nc-$Si_{0.9}Ge_{0.1}$ is faster than that of nc-Si. This is consistent with our previous results.[7,8] The decay curve is changed slightly by microcavity formation. The lifetime of nc-Si PL is shortened, while the lifetime of nc-$Si_{0.9}Ge_{0.1}$ is made longer. The time in which the PL intensity becomes $1/e$ of maximum intensity is 189.5 μs for nc-Si, and 90.5 μs for nc-$Si_{0.9}Ge_{0.1}$.

In a simple model, the spontaneous emission rate of a semiconductor $R_{sp}(\hbar\omega)$ is divided into an electric part $M(\hbar\omega)$ and a photonic part $G(\hbar\omega)$. [19] In principle, $M(\hbar\omega)$ is not changed by cavity formation. In the present samples, this is confirmed by measuring the PL spectrum from the cavity edge ($\theta=90°$). The spectrum from the cavity edge was almost the same as that of samples without the cavity structures.

In a microcavity, the electronic transition occurs only in the active layer. However, the optical mode, to which the excitonic transition couples, is extending into the DBR. As a result, the refractive index which affects $G(\hbar\omega)$ is not that of the active layer but an average of the refractive indexes of the layers in which the optical mode extends. Under the assumption that energy distribution of the optical mode falls monotonically, the penetration length (l_p) of the optical mode into a DBR is given by[20]

TABLE II. Optical mode extension into the distributed Bragg reflectors and effective refractive index (n_{eff}) for the various microcavities. Here, l_p^{top} and l_p^{bottom} are the penetration lengths on the surface side and on the substrate side, respectively, and τ_{cav} and τ_{act} are the PL lifetimes of the cavity and noncavity, respectively.

	l_p^{top} (nm)	l_p^{bottom} (nm)	n_{eff}	$(n_c/n_{\text{eff}})^3$	$\tau_{\text{cav}}/\tau_{\text{act}}$
nc-Si	255	269	1.93	0.68	0.93
nc-$Si_{0.9}Ge_{0.1}$	276	291	2.09	1.13	1.25

$$l_p=\frac{\lambda_c}{4n_c}\frac{q}{1-p}\frac{(1+a^2p^{m-1})(1-p^m)}{1+q^2a^2p^{2m-2}}, \tag{2}$$

where $q=n_c/n_L$, $p=n_L/n_H$, $a=n_H/n_{\text{sur}}$ or $a=n_H/n_{\text{sub}}$; whether the top DBR or the bottom DBR is considered, n_{sur} and n_{sub} are the refractive indexes of air and silicon dioxide, respectively, and m is the number of stacks in the DBR. The calculated penetration lengths (l_p^{top} and l_p^{bottom}) are summarized in Table II. The table shows that the optical mode is extended deeply into the DBRs.

The effective refractive index of the DBR (n_{DBR}) can be approximated by the spatial average between the high and the low refractive indexes, that is, $n_{\text{DBR}}=(n_Hl_H+n_Ll_L)/(l_H+l_L)$. The effective refractive index (n_{eff}) can be approximated by the average over the spatial extent of the optical mode:[16]

$$n_{eff}=\frac{n_{\text{DBR}}l_p^{\text{top}}+n_{DBR}l_p^{\text{bottom}}+\lambda_c}{l_p^{\text{top}}+l_p^{\text{bottom}}+\lambda_c/n_c}. \tag{3}$$

The n_{eff} calculated by this formula agrees very well with those estimated from Fig. 4. The important fact is that n_{eff} is larger than n_c for *nc*-Si, while n_{eff} is smaller than n_c for *nc*-$Si_{0.9}Ge_{0.1}$. The photonic part of the spontaneous recombination rate is proportional to the cube of the refractive index of the material (n^3). [19] If $M(\hbar\omega)$ is not changed by microcavity formation, the spontaneous recombination rate changes in proportion to n^3. In Table II, the values of $(n_c/n_{\text{eff}})^3$ and $\tau_{\text{cav}}/\tau_{\text{act}}$ are compared. We can see that the increase and decrease of τ_{cav} by microcavity formation for *nc*-$Si_{1-x}Ge_x$ and *nc*-Si can be qualitatively explained by the different dielectric contrast between the active layer and the DBRs. The quantitative disagreement may arise from oversimplification of the model and the fact that the PL lifetime reflects not only the radiative recombination process but also the nonradiative recombination processes. Nonradiative recombination processes are considered to be unaffected by microcavity formation.

IV. CONCLUSION

We studied the emission properties of *nc*-$Si_{1-x}Ge_x$ in Si/SiO_2 planar microcavity by measuring PL and time-resolved PL and comparing the results with those for *nc*-Si. We observed the commonly observed microcavity effects, that is, spectral narrowing, high directionality and enhancement of PL lines. In contrast to *nc*-Si, where the PL lifetime was shortened by microcavity formation, the PL lifetime of *nc*-$Si_{1-x}Ge_x$ became longer compared to the PL from a bare film. This result can be well explained by considering the difference in the dielectric contrast of active layer and that of DBRs into which an optical mode extends.

ACKNOWLEDGMENTS

This work was supported by a Grant-in-Aid for Science Research from the Ministry of Education, Science and Culture, Japan, and a Grant for Research for the Future Program from the Japan Society for the Promotion of Science (JSPS-RFTF-98P-01203). One of the authors (K.T.) would like to thank the Japan Society for the Promotion of Science.

[1] H. Takagi, H. Ogawa, Y. Yamazaki, A. Ishizaki, and T. Nakagiri, Appl. Phys. Lett. **56**, 2379 (1990).
[2] S. Schuppler, S. L. Friedman, M. A. Marcus, D. L. Adler, Y. -H. Xie, F. M. Ross, Y. J. Chabal, T. D. Harris, L. E. Brus, W. L. Brown, E. E. Chanban, P. F. Szajowski, S. B. Christman, and P. H. Citrin, Phys. Rev. B **52**, 4910 (1995).
[3] D. Kovalev, H. Heckler, G. Polisski, and F. Koch, Phys. Status Solidi B **215**, 871 (1999).
[4] Y. Kanzawa, T. Kageyama, S. Takeoka, M. Fujii, S. Hayashi, and K. Yamamoto, Solid State Commun. **102**, 533 (1997).
[5] M. Fujii, S. Hayashi, and K. Yamamoto, in *Recent Research Development in Applied Physics*, edited by S. G. Pandalai (Transworld Research Network, Trivandrum, 1998), Vol. 1, p. 193.
[6] S. Takeoka, M. Fujii, and S. Hayashi, Phys. Rev. B **62**, 16820 (2000).
[7] S. Takeoka, K. Toshikiyo, M. Fujii, S. Hayashi, and K. Yamamoto, Phys. Rev. B **61**, 15988 (2000).
[8] M. Fujii, D. Kovalev, J. Diener, F. Koch, S. Takeoka, and S. Hayashi, J. Appl. Phys. **88**, 5772 (2000).
[9] K. Toshikiyo, M. Tokunaga, S. Takeoka, M. Fujii, and S. Hayashi, J. Appl. Phys. **89**, 4917 (2001).
[10] K. Toshikiyo, M. Tokunaga, S. Takeoka, M. Fujii, S. Hayashi, and K. Moriwaki, J. Appl. Phys. **90**, 5147 (2001).
[11] S. Chan and P. M. Fauchet, Appl. Phys. Lett. **75**, 274 (1999).
[12] H. A. Lopez and P. M. Fauchet, Appl. Phys. Lett. **77**, 3704 (2000).
[13] F. Iacona, G. Franzo, E. C. Moreira, and F. Priolo, J. Appl. Phys. **89**, 8354 (2001).
[14] A. Serpenguzel and S. Tanriseven, Appl. Phys. Lett. **78**, 1388 (2001).
[15] A. M. Vredenberg, N. E. J. Hunt, E. F. Schubert, D. C. Jacobson, J. M. Poate, and G. J. Zydzik, Phys. Rev. Lett. **71**, 517 (1993).
[16] M. Cazzanelli and L. Pavesi, Phys. Rev. B **56**, 15264 (1997).
[17] H. R. Philipp, *Handbook of Optical Constants of Solids*, edited by E. D. Palik (Academic, New York, 1985), p. 765.
[18] N. E. J. Hunt and E. F. Schubert, *Microcavities and Photonic Bandgaps: Physics and Applications*, edited by J. Rarity and C. Weisbuch (Kluwer Academic, Dordrecht, 1995), p. 343.
[19] H. B. Bebb and E. W. Williams, *Semiconductors and Semimetals*, edited by R. K. Willardson and A. C. Beer (Academic, New York, 1972), Vol. 8, p. 181.
[20] D. I. Babic and S. W. Corzine, IEEE J. Quantum Electron. **28**, 514 (1992).